THE JOURNAL OF PHYSICAL CHEMISTRY B

Article

pubs.acs.org/JPCB

Molecular Dynamics Simulation Analysis of Anti-MUC1 Aptamer and Mucin 1 Peptide Binding

Kristen L. Rhinehardt, Goundla Srinivas, and Ram V. Mohan*

Department of Nanoengineering, Joint School of Nanoscience and Nanoengineering (JSNN), North Carolina A & T State University, 2907 E Lee St., Greensboro, North Carolina 27401, United States

Supporting Information

ABSTRACT: Aptasensors utilize aptamers as bioreceptors. Aptamers are highly efficient, have a high specificity and are reusable. Within the biosensor the aptamers are immobilized to maximize their access to target molecules. Knowledge of the orientation and location of the aptamer and peptide during binding could be gained through computational modeling. Experimentally, the aptamer (anti-MUC1 S2.2) has been identified as a bioreceptor for breast cancer biomarker mucin 1 (MUC1) protein. However, within this protein lie several peptide variants with the common sequence APDTRPAP that are targeted by the aptamer. Understanding orientation and location of the binding region for a peptide−aptamer complex is critical in their biosensor applicability. In this study, we investigate through computational modeling how this peptide sequence and its minor variants affect the peptide−aptamer complex binding. We use molecular dynamics simulations to study multiple peptide−aptamer systems consisting of MUC1 (APDTRPAP) and MUC1-G (APDTRPAPG) peptides with the anti-MUC1 aptamer under similar physiological conditions reported experimentally. Multiple simulations of the MUC1 peptide and aptamer reveal that the peptide interacts between 3′ and 5′ ends of the aptamer but does not fully bind. Multiple simulations of the MUC1-G peptide indicate consistent binding with the thymine loop of the aptamer, initiated by the arginine residue of the peptide. We find that the binding event induces structural changes in the aptamer by altering the number of hydrogen bonds within the aptamer and establishes a stable peptide−aptamer complex. In all MUC1-G cases the occurrence of binding was confirmed by systematically studying the distance distributions between peptide and aptamers. These results are found to corroborate well with experimental study reported in the literature that indicated a strong binding in the case of MUC1-G peptide and anti-MUC1 aptamer. Present MD simulations highlight the role of the arginine residue of MUC1-G peptide in initiating the binding. The addition of the glycine residue to the peptide, as in the case of MUC1-G, is shown to yield a stable binding. Our study clearly demonstrates the ability of MD simulations to obtain molecular insights for peptide−aptamer binding, and to provide details on the orientation and location of binding between the peptide−aptamer that can be instrumental in biosensor development.

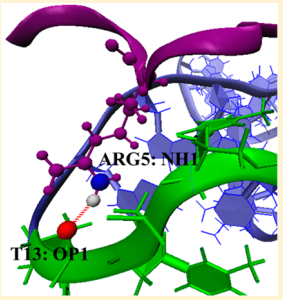

INTRODUCTION

Biomarkers are molecules linked to changes in concentration, physiology, and morphology within an organism.[1] These molecules are effective sources as discerning diagnostic tools for detecting and tracking disease progression. Recently, developments in biosensors have garnished a lot of interest in cancer research for their unique applications as diagnostic devices.[2−11] At the genetic level, a prevalent gene associated with breast cancer is the mucin 1 (MUC1) gene.[12] The MUC1 gene encodes transmembrane mucin proteins.[13] In breast carcinomas the MUC1 protein is no longer transmembrane, but rather up-regulated and free floating in the bloodstream.[13] The carcinogenic isoform of these proteins lack the tandem repeat regions[12,13] and have shortened O-glycan's which expose a variety of peptide epitopes.[14−16] Mucin 1 peptides often contain the sequence APDTRPAP. The SM3 antibody has a high affinity for this cancerous isoform of MUC1[13,17,18] and has been crystallized with the peptide antigen APDTRPAP.[14] The concentration of the MUC1 isoform can be related to disease severity[13,19] which could be detected and assessed within a biosensor.

A biosensor is a receptor-transducer device that provides quantitative information using a bioreceptor and a transducer.[20] Generally a transducer is based on electrochemical, mass, optical, or thermal changes while the bioreceptor acts on biochemical recognition.[20,21] When a biological sample is introduced into the sensor, the bioreceptor targets its desired ligand in the sample and binds to it. The change of state due to the interaction of the bioreceptor and ligand is registered and quantified by the transducer. Selecting efficient bioreceptors presents a major challenge for biosensor development.[20] Antibodies are large biomolecules commonly used bioreceptors.[22] Despite their use, antibodies are not always easily synthesized, can be chemically unstable thus limiting their application to single use biosensors.[23] The large size of the antibodies often limits their application to low density biosensors.[23,24]

Received: March 13, 2015
Revised: May 8, 2015

DOI: 10.1021/acs.jpcb.5b02483
J. Phys. Chem. B XXXX, XXX, XXX−XXX

Such limitations and difficulties with antibodies motivated the search for efficient alternative biorecognition elements. Studies have shown that aptamers can be potential bioreceptors.[22,23,25−27] Aptamers are broadly considered as single stranded DNA or RNA oligonucleotide.[28] Aptamers are relatively small, chemically stable biomolecules and have a high binding affinity that rival or better than that of antibodies. These properties make aptamers advantageous as bioreceptors.[28] Sequence level binding as well as their ability to undergo changes in conformation upon binding contributes to the high binding affinity of aptamers. In addition, aptamers are readily functionalized and immobilized on a surface creating highly ordered receptor layers.[20]

Because of the complexity and vast possibilities of combinations, RNA and DNA oligonucleotides have been compiled into aptamer libraries. For example, a standard 25-mer library compilation has 10^{15} available aptamers.[29] Clearly, selecting an appropriate aptamer from such a large pool is not practical. In 1990, the SELEX (systematic evolution of ligands by exponential enrichment) process provided an experimental solution for aptamer selection. In this process, several smaller pools of developed aptamer libraries undergo incubation with the desired target molecule.[29,30] Successfully bound aptamers from the incubation process are enhanced through polymerase chain reactions (PCR);[31−33] the incubation and subsequent steps are repeated to generate a select assembly of high affinity aptamers.[30,34] Upon completion of the SELEX cycle, these high affinity aptamers are sequenced to uncover their makeup.

After successful selection and sequencing of an aptamer, it needs to be immobilized in the biosensor. The method of immobilization[35] and orientation of the aptamer within a biosensor directly affects its efficiency.[36−38] Biosensor efficiency is greatly increased when the biorecognition element is oriented in such a way that the binding site is easily accessible.[35,38] Experimental studies have shown that the anti-MUC1 aptamer binds to the mucin 1 protein, in particular the exposed peptide epitopes that distinguish this carcinogenic isoform.[39] Isolating and understanding peptide mechanisms and actions can provide key information on the larger proteins they embody.[40] Given that these peptide epitopes are the targets of the aptamer, they can be used in lieu of the proteins for experimentation.[39] However, details of binding process including the aptamer orientation and location of binding between unbound MUC1 peptides and the aptamer are not known. Such details about the aptamer configuration are important in the function of an aptamer-based biosensor as small changes in conformation or structure can have significant effects on the detection capability of the biosensor.[39,41,42] Molecular level insights into such a complex phenomenon can be achieved with the aid of suitable computational modeling to improve our understanding of aptamer binding.

In this work, computational modeling is employed and shown to be an avenue to test, analyze, and visualize the progression of the peptide−aptamer binding. In particular, as discussed before, binding is the foundation for the aptamer selection process and biosensor detection. Molecular dynamics is a computational methodology commonly used to study many biomolecules.[40,43−45] A detailed molecular dynamics modeling analysis of individual MUC1 peptide, MUC1-G peptide, and anti-MUC1 aptamer systems in solvent and their interactions are presented and discussed in the present paper. A preliminary study of molecular dynamics modeling was previously discussed for a similar system based on MUC1 peptide.[46]

Modeling of the natural progression of peptide−aptamer binding in a solvent identifies key features such as orientation and location of the aptamer in the binding event, thus providing insights for biosensor development. A series of extensive molecular dynamics (MD) simulations of MUC1 and MUC1-G peptides and aptamer combinations in solvent were conducted. Quantification of the results defining the specifics of aptamer-peptide binding and their relevance in biosensor development are discussed.

II. METHODS

The atomistic representation of MUC1 aptamer was used in the present computational modeling study. Initial configurations for the biomolecules studied were obtained from the protein data bank. The 115 atom MUC1 peptide sequence APDTRPAP (shown in Figure 1A) was isolated from the antibody complex using the visualization and analysis software Pymol.[47] In order to create a variant of the MUC1 peptide, the MUC1 sequence was further modified by adding a glycine residue forming the MUC1-G peptide (APDTRPAPG) with 122 atoms (shown in Figure 1B). The NMR structure of the S2.2 anti-MUC1 aptamer contained 728 atoms (Figure 1C). This aptamer has a net charge of −22.0 units of electric charge (e). Pymol was used to create the initial configurations of the MUC1 peptide−aptamer and MUC1-G peptide−aptamer molecular systems by combining the original PDB files.

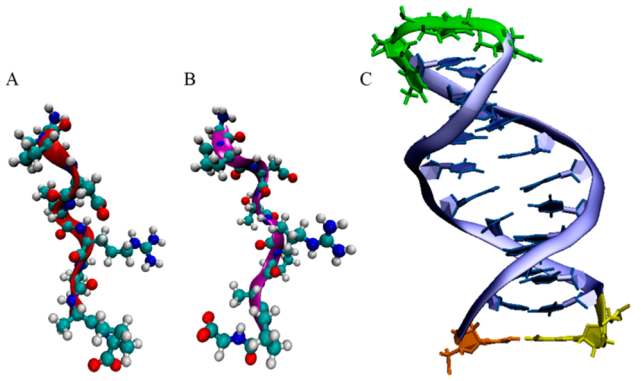

Figure 1. Structures of molecules used in the present study are shown: (A) MUC1 peptide (B) MUC1-G peptide and (C) anti-MUC1 S2.2 23-mer Aptamer with the 3′ (highlighted in orange) and 5′ (highlighted in yellow) ends illustrated along with the open loop region of the aptamer consisting of 3 thymine nucleotides (highlighted in green). In parts A and B, peptide backbones are represented in ribbon format, while the side chains are shown in a ball and stick representation. Color code: oxygen, red; carbon, cyan; nitrogen, blue; hydrogen, white. In part C, nucleic acids are shown as a ribbon backbone.

Detailed molecular dynamics simulations, using the structures shown in Figure 1, were conducted with the Amber99sb force field[48] using GROMACS, an open source efficient MD code that is commonly used to simulate complex biological systems.[49] This force field has been shown to be effective in protein modeling and used in several molecular dynamics simulations of DNA.[50−53] Initially, individual simulations of the MUC1 peptide, MUC1-G peptide, and anti-MUC1 aptamer in solvent were conducted. Subsequently, the peptide−aptamer combinations in solvent were simulated. In all the simulations we considered a 0.15 M NaCl solvent at the room temperature (300 K) and the atmospheric pressure (1 bar) to closely mimic

DOI: 10.1021/acs.jpcb.5b02483
J. Phys. Chem. B XXXX, XXX, XXX−XXX

Table 1. Simulation Details for Individual Molecules and Aptamer−Peptide Complexes in Solvent

	system	box volume (nm^3)	salt concentration (M)	number of atoms in the biomolecules	number of Na^+ ions	number of Cl^- ions	water molecules	simulation time (ns)
individual molecule simulations	MUC1 aptamer	398.89	0.15	728	58	36	12741	10
	MUC1 peptide	146.43	0.15	115	13	13	4792	10
	MUC1-G peptide	120.56	0.15	122	11	11	3957	10
aptamer−peptide complex simulations	MUC1 peptide and aptamer[b]	465.48	0.15	843	64	42	15158	250
	$MUC1_1$ peptide and aptamer[b]	1043.43	0.15	843	116	94	34085	300
	$MUC1_2$ peptide and aptamer[b]	650.48	0.15	843	82	59	21191	300
	MUC1-G peptide and aptamer	1138.77	0.15	850	125	103	37356	300
	$MUC1\text{-}G_1$ peptide and aptamer[a]	416.77	0.15	850	60	38	13423	300
	$MUC1\text{-}G_2$ peptide and aptamer[a]	363.66	0.15	850	55	33	11711	300
	$MUC1\text{-}G_3$ peptide and aptamer[a]	873.46	0.15	850	101	79	28509	300

[a]The simulations involving $MUC1\text{-}G_1$, $MUC1\text{-}G_2$, and $MUC1\text{-}G_3$ are similar to that of MUC1-G, except they have different starting configurations. [b]The simulations involving $MUC1_1$ and $MUC1_2$ are similar to that of MUC1, except they have different starting configurations.

the general experimental conditions. In order to neutralize the aptamer, 22 Na^+ ions were added to the simulation system.

During MD analysis, each biomolecule was minimized to provide a minimal energy configuration using steepest descent technique and the potential energy was carefully analyzed to ensure the simulation system reached a stable configuration. This minimized structure was further equilibrated using *NVT* and *NPT* thermodynamic state ensembles. The *NVT* thermal equilibration was done with a constrained structure and a velocity rescale thermostat specific to GROMACS.[54,55] Subsequently, *NPT* pressure equilibration was applied with the same velocity-rescale temperature coupling in addition to the Parrinello−Rahmen pressure coupling.[56] The fully temperature and pressure equilibrated system was then used as the initial configuration for the MD production dynamic analysis. During dynamic analysis, all the atoms were unconstrained and free to move in their most energetically favorable positions. All simulations were conducted using a 2 fs time step. Individual biomolecular simulations of the aptamer and peptides were conducted for a time period of 10 ns to establish their molecular behavior. Later, in order to verify the robustness of the results multiple simulations of the MUC1 peptide−aptamer and MUC1-G peptide−aptamer combinations were conducted for a minimum of 250 ns following the same MD procedure. Initial configurations for these simulations differ from each other. Nevertheless, they all have the same molar concentration of NaCl (0.15M) which is determined as follows.

$$\text{number of } Na^+ \text{ ions} = \text{number of } Na^+ \text{ ions needed for neutralization} + \text{number of } Na^+ \text{ ions for the corresponding salt concentration}$$

$$\text{number of } Cl^- \text{ ions} = \text{number of } Cl^- \text{ ions for the corresponding salt concentration}$$

$$\text{number of } Na^+ \text{ ions} = 22 + \left\lceil (6.023 \times 10^{23}\ \text{mol}^{-1}) \times \text{box volume nm}^3 \times 0.15\frac{\text{mol}}{\text{L}} \right\rceil$$

$$\text{number of } Cl^- \text{ ions} = \left\lceil (6.023 \times 10^{23}\ \text{mol}^{-1}) \times \text{box volume nm}^3 \times 0.15\frac{\text{mol}}{\text{L}} \right\rceil$$

All simulations were performed at standard temperature (300 K) and pressures (1 bar) in 0.15 M NaCl solvent environment. The number of Na^+, Cl^- ions and water molecules along with the corresponding box volumes for all simulation systems are listed in Table 1.

Following the simulation, final configurations of the molecular systems were examined for any structural reorganization using visual molecular dynamics (VMD) software and GROMACS.[57] In order to analyze and quantify peptide−aptamer binding, distance between the aptamer and peptide atoms, root-mean-square deviation (RMSD),[58] radius of gyration (R_g)[59] and the number of hydrogen bonds were analyzed.

III. RESULTS

A. Simulations of Individual Molecules in Solvent. Individual biomolecular system simulations give insight into the possible conformations and identify potential binding sites. Simulation snapshots of the individual MUC1 aptamer and peptides are shown in Figure 2. The peptide showed little change in the conformation during the initial stages of transient dynamic simulation. However, its conformation significantly altered as the simulation and transient time proceeded. It was observed that in the initial stages of simulation, peptide structure became compact but in the later stages the structure returned to a conformation similar to that of the starting structure (Figure 2A). Furthermore, the peptide frequently altered its conformation during the simulation due to the flexible nature of the backbone. Conversely, the addition of the

DOI: 10.1021/acs.jpcb.5b02483
J. Phys. Chem. B XXXX, XXX, XXX−XXX

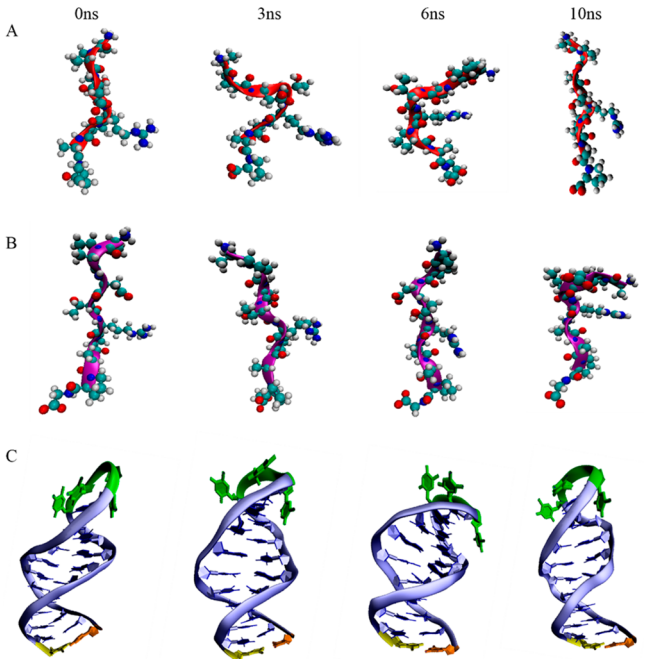

Figure 2. Snapshots at 0, 3, 6, and 10 ns obtained from MD simulations of (A) MUC1 peptide (B) MUC1-G peptide, and (C) anti-MUC1 aptamer are shown. Water and ions are not shown for figure clarity.

glycine residue in the MUC1-G peptide was found to decrease the flexibility of the backbone. For this reason, the backbone appeared to be less flexible compared to the MUC1 peptide although it has free rotational motion (Figure 2B). However, the addition of the glycine does not make the peptide completely rigid, which was evident in the later stages of the transient dynamic simulation analysis.

Unlike the peptides, the aptamer structure showed little or no change during the transient dynamic simulation. MD analysis results revealed two distinct open regions within the aptamer where binding may occur. The first being the loop region of the aptamer that has three nonbase paired thymine nucleotides and the second open region include the 3′ and 5′ ends (highlighted regions in Figure 1C). Simulation also showed rotation of the three thymine nucleotides in the loop and relatively less mobility of the nucleotides at the open ends (Figure 2C).

In order to investigate the conformational changes, we calculated the structural quantities such as RMSD and R_g for the aptamer and peptides as shown in Figure 3. The RMSD and R_g of the MUC1 peptide showed a significant variation throughout the simulation (Figure 3). The flexible backbone of the peptide causes large fluctuations as atoms rattle and shift in the confined space. The changes observed in the backbone movement are also reflected in the RMSD values which fluctuated between 0.12 and 0.44 nm as shown in Figure 3A. The flexibility of the peptide backbone is evident from the fluctuations in R_g as well (Figure 3B).

The addition of the glycine residue in the variant MUC1-G peptide illustrated minor differences in structural behavior compared to the MUC1 peptide. Overall, the MUC1-G peptide showed a reduction in fluctuations in the R_g and RMSD (Figure 3). Despite this reduction the MUC1-G peptide is still capable of obtaining the conformations mirrored by the MUC1 peptide. The higher RMSD values seen in Figure 3A for the MUC1-G peptide compared to that of MUC1 peptide can be attributed to the addition of the glycine residue. Similarly, the starting value of R_g of 0.8 nm for the MUC1-G peptide was higher than that of the MUC1 peptide, which can also be attributed to the addition of this glycine residue. Later stages of simulations indicated that the peptide obtains a more compact motif resulting in a steep reduction in the R_g (Figure 3B).

The aptamer showed significantly different structural behavior compared to the peptides. The RMSD of the aptamer initially was at 0.25 nm. Throughout the dynamic simulation, the RMSD fluctuates before stabilizing to a value around 0.18 nm (Figure 3A). This can be attributed to the flexible movement of the thymine nucleotides in the loop region. The R_g value for the aptamer was found to be consistently around 1.3 nm (Figure 3B). This demonstrates that the aptamer has a relatively stable structure with little variation.

B. MD Analysis of Peptide−Aptamer Interactions. *I. MUC1 Peptide−Aptamer Simulations.* After establishing the individual biomolecule behavior, we proceed to examine the peptide−aptamer systems. Snapshots from the molecular dynamics simulation of the initial peptide−aptamer combination are shown in Figure 4. During the simulation the aptamer and MUC1 peptide move apart compared to their initial configuration (Figure 4A). During the initial stages of the MD progression, the peptide associated briefly with the 12th thymine nucleotide in the aptamer loop (Figure 4B). The peptide then was found to disassociate before a quick

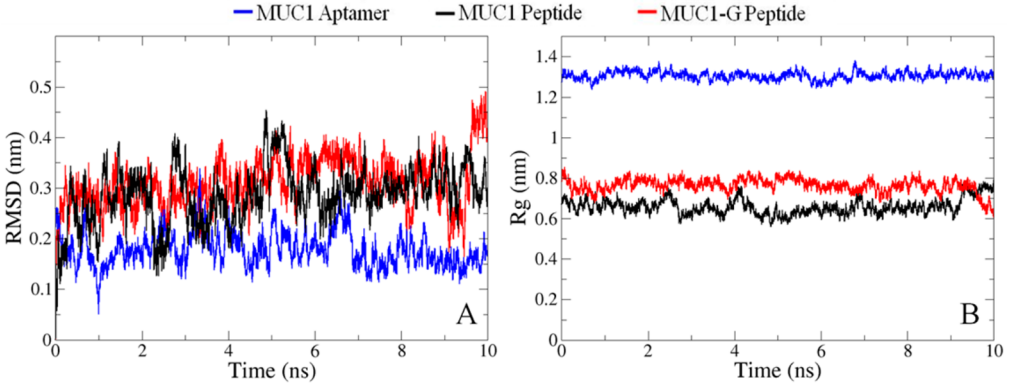

Figure 3. Structural analysis of MUC1 peptide (black), MUC1-G peptide (red) and anti-MUC1 aptamer (blue), obtained from individual biomolecule simulations in solvent. (A) RMSD and (B) R_g during 10 ns simulation are plotted.

DOI: 10.1021/acs.jpcb.5b02483
J. Phys. Chem. B XXXX, XXX, XXX−XXX

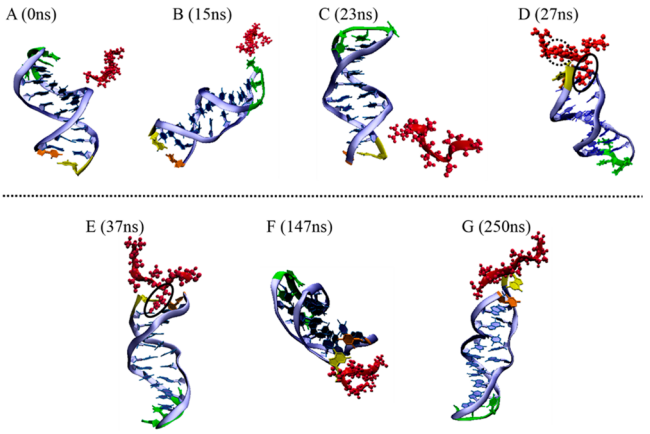

Figure 4. Anti-MUC1 aptamer (blue backbone) and MUC1 peptide (red backbone and residues) snapshots as observed in a 250 ns MD simulation are shown (without water or ions). (A) Starting structure. (B) Brief association event of aptamer–peptide. (C) Dissociation of the aptamer and peptide. (D) Initial association between the arginine residue (circled in solid line) and aspartic acid residue (circled in dashed line) of the peptide backbone and 5′ end (yellow) of the aptamer. (E) Peptide–aptamer snapshot taken at 10 ns after initial association. (F) Peptide–aptamer snapshot 120 ns after the initial association. (G) Peptide–aptamer combination at 250 ns.

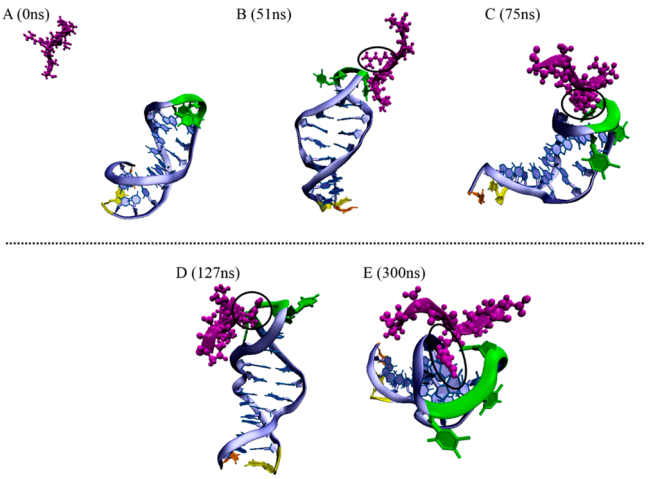

Figure 5. Anti-MUC1 aptamer (blue backbone) and MUC1-G peptide (purple backbone and residues) snapshots obtained from a 300 ns MD simulation are shown (without water or ions). (A) Initial peptide–aptamer configuration. (B) Initial interaction of the aptamer and the arginine residue of the peptide (circled in black). (C) Peptide–aptamer association between the open loop region of the aptamer and the arginine residue of the peptide at 25 ns after initial association. (D) Peptide–aptamer conformation at 76 ns after association. (E) Peptide–aptamer conformation at the end of the 300 ns simulation.

reassociation (aided by aspartic acid and arginine residues of the peptide) with the 5′ end of the aptamer (Figure 4C,D) in a parallel conformation to that of the aptamer. However, after 10 ns of association the peptide deviates from its parallel orientation. Interestingly, the arginine residue of the peptide (5th residue in the peptide sequence) still appears to be interacting with the aptamer at this stage (Figure 4E). Extending the MD simulation analysis to 250 ns showed the peptide continued to remain near the 5′ and 3′ open ends of the aptamer (Figure 4F,G). In order to ascertain if this is a consistent behavior, multiple simulations with different initial configurations of MUC1 peptide–aptamer combinations were carried out (see Table 1). In each simulation we observe brief association events similar to the described results (detailed results are shown in the Supporting Information).

II. MUC1-G Peptide–Aptamer Simulations. Snapshots from the simulation of the initial MUC1-G peptide–aptamer combination are shown in Figure 5. Analysis show that the MUC1-G peptide–aptamer combination exhibits markedly different structural behavior from that of the MUC1 peptide–aptamer combination. The addition of the glycine residue to the peptide caused significant changes in MUC1-G peptide–aptamer behavior. Unlike the MUC1 combination, the peptide in MUC1-G associated with the open loop region of the aptamer in this case (Figure 5B). The arginine residue of the peptide was found to interact with the 11th and 13th thymine nucleotides of the aptamer (Figure 5C). Extended simulation to 300 ns, reveal a continuous association between the aptamer and peptide. As before, this was confirmed by carrying out multiple simulations with different initial configurations of MUC1-G peptide–aptamer combinations (see Table 1).

C. Comparative Quantitative Analysis. It was not always clear from the visual analysis if the peptide and aptamer were in a bound configuration or in the physical vicinity of the binding regions. In order to elucidate the occurrence of peptide–aptamer binding we carried out detailed quantitative analysis. The calculated distribution of ions, center of mass distance, and distance between the atoms within binding region for both MUC1 and MUC1-G peptide complexes are shown in Figure 6. These analytical quantities together help monitor and quantify binding events.

As the aptamer carries additional charge it is important to monitor the distribution of ions around peptide–aptamer complex during the simulation. The average distribution of number of ions around the MUC1 and MUC1-G complexes obtained by computing the radial distribution function (RDF) is shown in Figure 6A. It is clear that there are two distinct distances, 0.25 and 0.4 nm, where the ions have a relatively higher presence near the surface of the molecules. The results also show that the presence of ions is slightly higher around the MUC1-G peptide compared to that of MUC1 peptide.

In order to verify the binding event the distance between the peptide and the aptamer was evaluated by considering the center of mass (COM) of the individual biomolecules. The distance between the aptamer and peptide COM was found to decrease and remain consistently near 2 nm in both MUC1 and MUC1-G peptide–aptamer combinations (Figure 6B). In order to further ascertain if the aptamer and peptide are in fact binding, the distance between the aptamer and peptide atoms that are specific to the binding region were calculated and analyzed. The binding region was defined by analyzing the final binding configurations of the peptide–aptamer systems and identifying the atoms specifically and consistently involved in binding (atoms used in this analysis are listed in the Supporting Information). A successful peptide–aptamer binding is known to be noncovalent consisting of hydrogen bonds, van der Waals forces and electrostatic interactions.[60,61] van der Waals interactions play significant role in such noncovalent binding, which typically extend to a distance of 0.6 nm for large biomolecules. In the present simulation systems, we conservatively used a distance of 0.45 nm as the cutoff distance to define noncovalent peptide–aptamer binding.[61−63] Accordingly, the peptide–aptamer combination was considered to be

DOI: 10.1021/acs.jpcb.5b02483
J. Phys. Chem. B XXXX, XXX, XXX−XXX

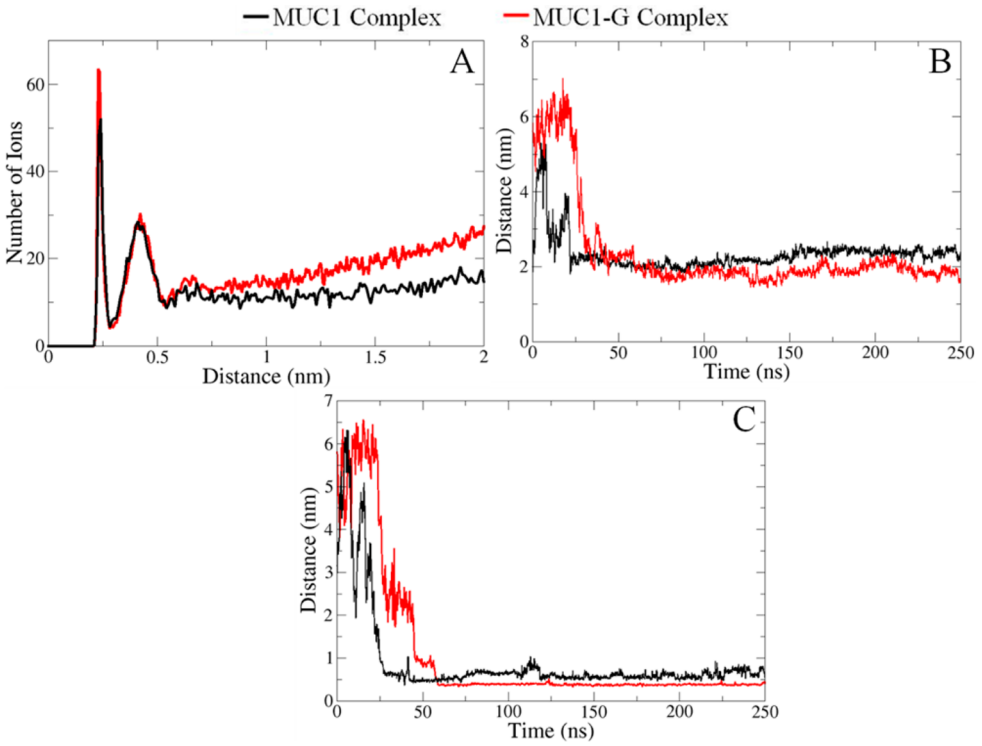

Figure 6. Comparison of anti-MUC1 aptamer binding with MUC1 peptide (black) and MUC1-G peptide (red). (A) Distribution of average number of ions around the peptide−aptamer complex. (B) Center of mass distance of the aptamer and peptide molecules. (C) Distance between the atoms within the binding region of the aptamer and peptides.

bound if the distance between the atoms within the binding region is less than 0.45 nm for a minimum of 15 ns.

As stated previously, the MUC1 peptide and aptamer combination visually showed the formation of a peptide−aptamer complex (Figure 4D). The simulation trajectory analysis shows that the distance between the binding atoms of the MUC1 peptide−aptamer combination falls below 0.45 nm briefly (for less than 1 ns) during the simulation (Figure 6C). As the simulation continued this distance increases and remains above 0.45 nm indicating that the MUC1 peptide and aptamer molecules were not in a bound configuration. Also, the distance values were consistently closer to 0.6 nm which is the upper threshold used for large biomolecules.[61] Continued simulation to 250 ns showed the distance between the aptamer and MUC1 peptide was 0.6 nm and higher (Figure 6C), thus confirming this to be a nonbinding complex. Unlike the MUC1 peptide−aptamer combination, simulations of MUC1-G peptide−aptamer combination exhibit a strikingly different behavior. The distance between the atoms in the binding region in this case falls below 0.45 nm during the initial association and remains below this threshold for the remainder of the simulation (Figure 6C). The atoms in the binding region of the MUC1-G peptide−aptamer complex averaged a distance of 0.39 nm after initial association. This clearly indicates that the MUC1-G peptide and aptamer bind and remain in that conformation throughout the simulation. This sustained binding was consistent in all cases with varying starting configurations of MUC1-G listed in Table 1. This is discussed further in the next section.

D. Multiple MUC1-G Peptide-Aptamer Simulations. Wet lab experiments with a variety of MUC1 peptides have shown that the MUC1-G peptide−aptamer combination has a higher binding affinity and is the most favorable binding combination.[39] Our simulations and analysis discussed earlier support these findings as binding occurred only with the MUC1-G peptide−aptamer combination. In order to further validate the consistency and repeatability of MUC1-G peptide−aptamer binding, we have carried out multiple additional simulations of this combination in solvent. For this purpose, we constructed three additional MUC1-G peptide−aptamer systems under the same physiological conditions as described before (Table 1). These complexes are represented as MUC1-G_1, MUC1-G_2, and MUC1-G_3 with varying initial conformations (details on the structural set up for each peptide aptamer combination are found in the Supporting Information). Each of these simulations was carried out for at least 300 ns.

The binding event in all cases was examined by calculating the distance between the aptamer and MUC1-G peptide atoms in the binding region. Simulations show that these combinations varied in binding time but indicated consistent and sustained binding of MUC1-G peptide with the loop region of the aptamer as before. The binding conformation of the peptide in the loop region slightly differed for each of these three MUC1-G peptide−aptamer combinations. Snapshots of the binding events from each of these simulations are shown in Figure 7. Together these simulation results indicate the consistency and repeatability of the MUC1-G peptide−aptamer binding event. All the simulations indicate that the arginine residue consistently plays an integral role in the binding. The orientation of the peptide differs in each binding event, but the location in the loop region is consistent. The interaction between the arginine residue and the 13th thymine nucleotide is predominantly present in all the three binding complexes studied. In one particular case (MUC1-G_3), in addition to arginine, an adjacent proline residue of the peptide was also found to interact with the 13th thymine nucleotide. In this case,

DOI: 10.1021/acs.jpcb.5b02483
J. Phys. Chem. B XXXX, XXX, XXX−XXX

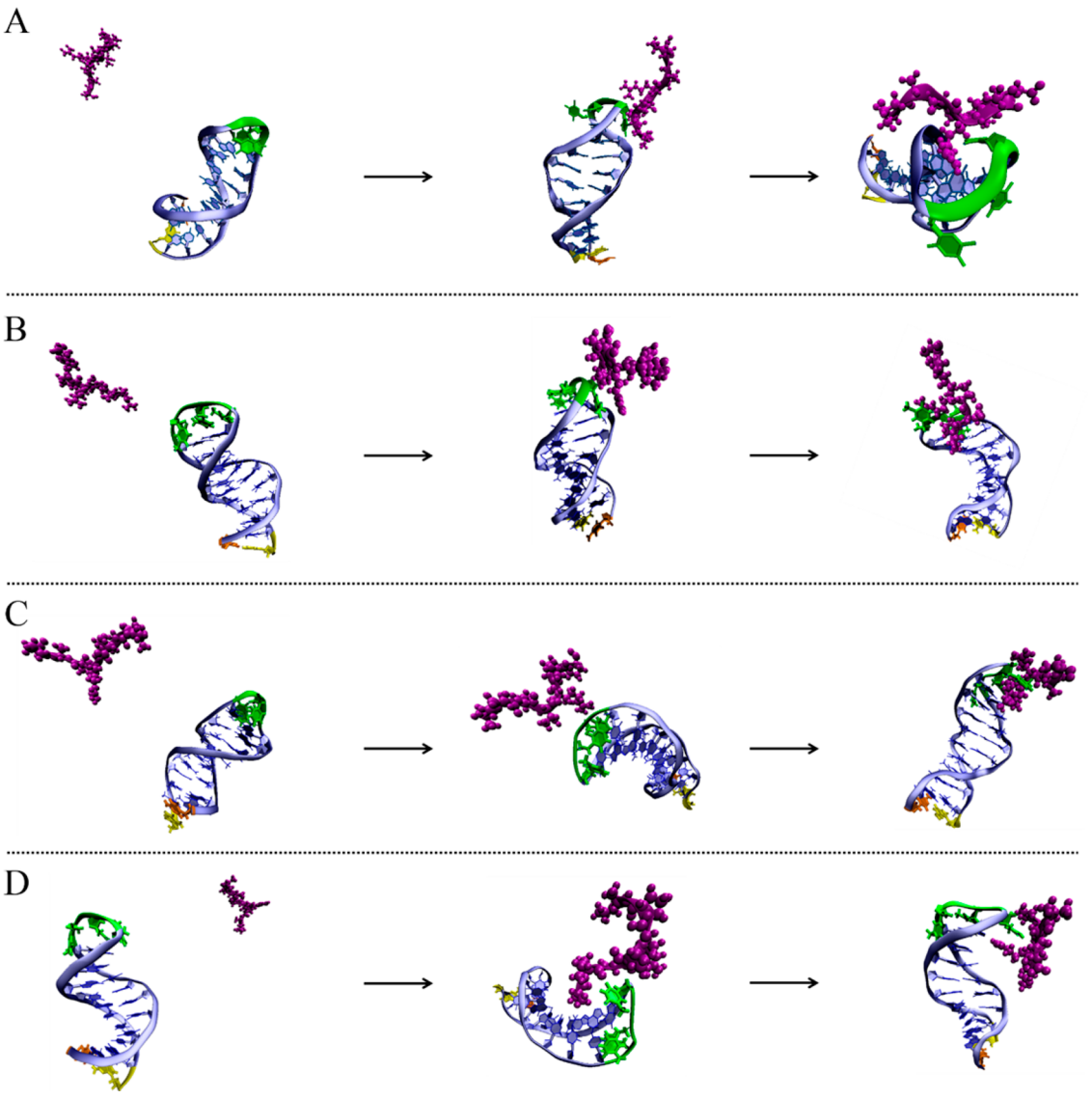

Figure 7. Simulation snapshots of initial, binding and final configurations (shown without water or ions for clarity). (A) MUC1-G, (B) MUC1-G_1, (C) MUC1-G_2, and (D) MUC1-G_3.

detailed visual analysis shows that the peptide backbone in the MUC1-G_3 case forms an arc-like conformation (which was not observed in the other cases) around the loop. We find that this conformational change facilitates the proline residue interaction with the 13th thymine nucleotide contributing to a stable binding conformation (Figure 7D).

We again examined the distribution of ions in each simulation around these aptamer and peptide molecules (Figure 8). By computing the radial distribution function (RDF) of the Na^+ and Cl^- around the aptamer and peptide we found that the first major peak occurs at 0.25 nm, followed by second and third peaks around 0.4 and 0.6 nm as shown in Figure 8A. Examination of the distribution of individual ions show that the Na^+ ions are predominant contributors to the ion distributions as revealed by their presence at 0.25 and 0.4 nm (shown in Figure 8B). This is expected as the DNA is negatively charged and would be attracted to the Na^+ ions. On the other hand, negatively charged Cl^- ions are not found near the aptamer surface but their presence gradually increases away from the surface (Figure 8C).

Prior discussions clearly establish the consistent occurrence of binding in all MUC1-G cases. This was also reflected in the quantitative comparative analysis of the structural quantities. We observed that the radius of gyration (R_g) for all MUC1-G peptide−aptamer simulations show similar behavior. R_g for each MUC1-G aptamer-peptide complex are presented in the Supporting Information. Figure 9 shows the distribution of the R_g for the initial (blue) and final (red) 1 ns interval of MUC1-G peptide and aptamers from all the simulations. The initial configurations show a widespread of R_g values. Though the time for the binding event varied in each case, after the binding event all the R_g values converged to a value of 1.4 nm as shown in Figure 8. The convergence of the R_g further substantiates the consistency and repeatability of the MUC1-G binding.

Figure 10 shows the average COM distance and binding atom distance results at key time intervals in the simulation. The average distance values are shown with symbols along with the corresponding variations calculated for the 4 MUC1-G simulations. Both the distance values and variations progressively decrease and converge with the binding event. We find that in all the simulations the COM distance between the

DOI: 10.1021/acs.jpcb.5b02483
J. Phys. Chem. B XXXX, XXX, XXX−XXX

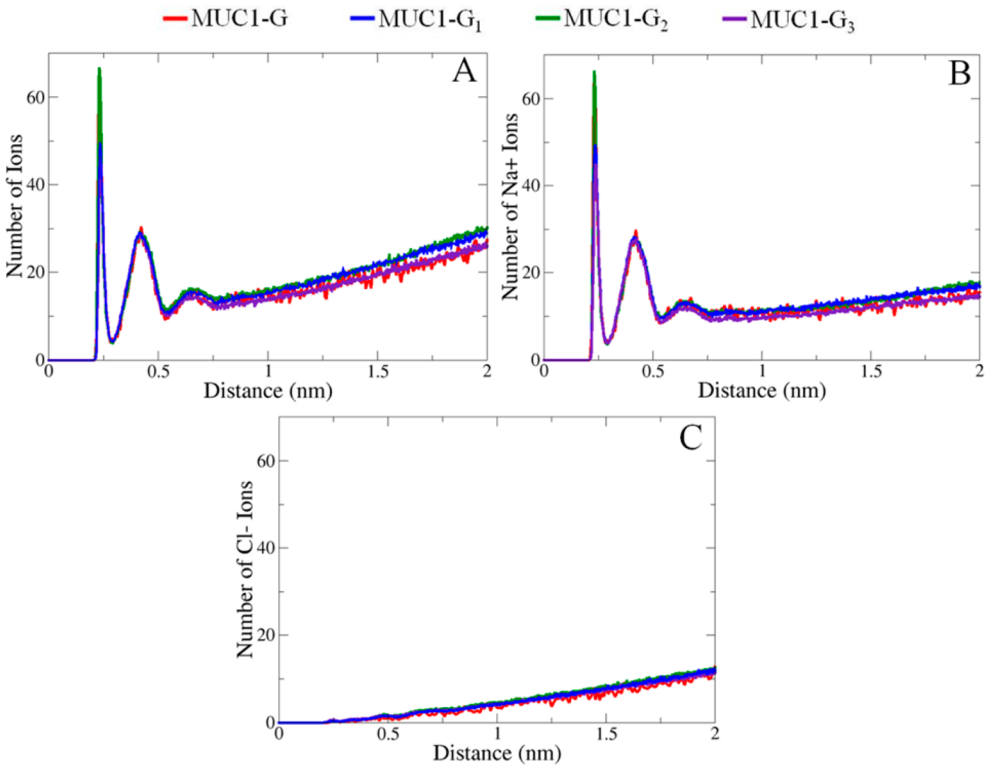

Figure 8. Average distribution of ions around the MUC1-G complexes. (A) Distribution of NaCl ions. (B) Distribution of Na^+ ions. (C) Distribution of Cl^- ions. Note: MUC1-G (red). MUC1-G_1 (blue), MUC1-G_2 (green), and MUC1-G_3 (purple).

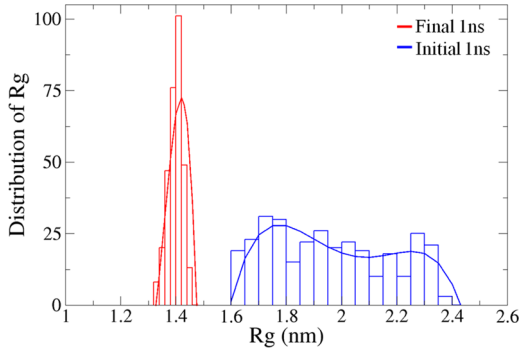

Figure 9. Distribution of the radius of gyration of MUC1-G peptide–aptamer combinations for the initial (blue) and final (red) nanosecond of all MUC1-G peptide and aptamer simulations. Corresponding polynomial fits for the distributions are shown as lines.

MUC1-G peptide and aptamer converged to a value of at least 2 nm after the binding (Figure 10A). Although each simulation was started with a different initial configuration for peptide–aptamer combination, we observe successful and sustained binding in every case. This is also confirmed by calculating the distance between the atoms in the binding region of the peptide–aptamer complex, which converged to a distance below the considered binding threshold distance of 0.45 nm. The average binding atom distance exhibits minimal variation after the binding event as shown in Figure 10B. Together these results indicate the consistency and repeatability of the MUC1-G peptide–aptamer sustained binding.

Figure 11 shows the distribution of the distances for the initial (blue) and final (red) 1 ns interval of MUC1-G peptide and aptamers from all the MUC1-G simulations. As can be seen from the figure, the distributions corresponding to starting configurations are relatively wide. This is due to the fact that the initial configurations of the peptide and aptamer structures were created to be separated by a minimum distance of 3 nm. On the other hand, the distances corresponding to the final configurations show a narrower distribution centered around a distance of 2 nm with a significantly smaller spread compared to the initial distribution (Figure 11A). We further analyze the distribution of the distances between the atoms in the binding region alone (shown in Figure 11B). The distribution of the binding atoms in the initial 1 ns configurations is similar to the COM distances. However, the final nanosecond of simulation show a much narrower distribution centered around a value of 0.3 nm which is well below the binding threshold distance of 0.45 nm considered in this study. Together, these distributions show that the initially well separated MUC1-G peptide and aptamer molecules successfully and consistently bind.

E. Hydrogen Bonding Analysis. From the simulation snapshots (shown in Figure 7), it is apparent that the aptamer undergoes structural reorganization during the MUC1-G binding event. Hydrogen bond analysis could identify such structural changes,[64] since the aptamer tertiary structure is held together by the formation of hydrogen bonds. Figure 12 shows the average number of intramolecular hydrogen bonds for all MUC1-G peptide and aptamer combinations at key intervals (see Supporting Information for a comparison of the number of hydrogen bonds in MUC1 and MUC1-G complexes). Consistent with the GROMACS analysis, we consider the hydrogen bonds to have a maximum distance of 0.35 nm and a corrresonding angle of 30° or less between the donor and acceptor atoms.[65] In all cases at the start of the simulation several hydrogen bonds were found to hold the structure together except in the loop and helical regions of the aptamer. As the simulation continues we observe an increase in the

DOI: 10.1021/acs.jpcb.5b02483
J. Phys. Chem. B XXXX, XXX, XXX–XXX

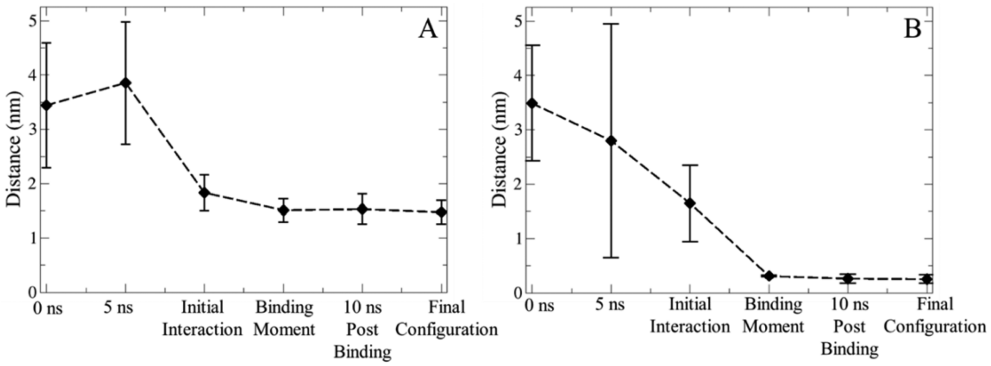

Figure 10. Distance plots at significant times in the binding simulations of multiple MUC1-G peptide−aptamer combinations. The average distance values are shown as symbols along with corresponding variations. (A) COM distance and (B) Binding atom distance. As can be seen from the figures, both the distance values and variations progressively decrease and converge with the binding event.

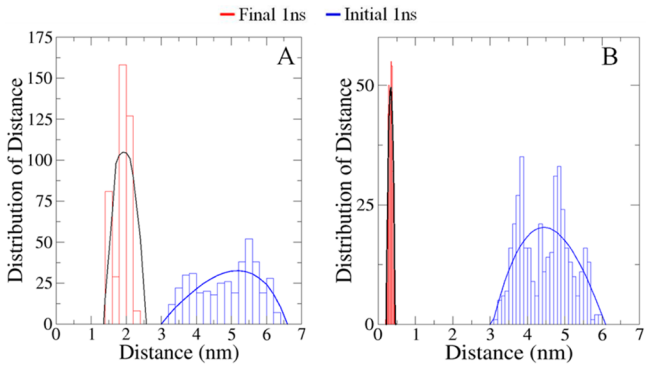

Figure 11. Distance distributions for the initial (blue) and final (red) nanosecond of all MUC1-G simulations. (A) Distance distribution between the COM of MUC1-G peptide and aptamer and (B) distance between the atoms within the binding region of the MUC1-G peptide and aptamer combination. Polynomial fits obtained for the corresponding distributions are shown as lines.

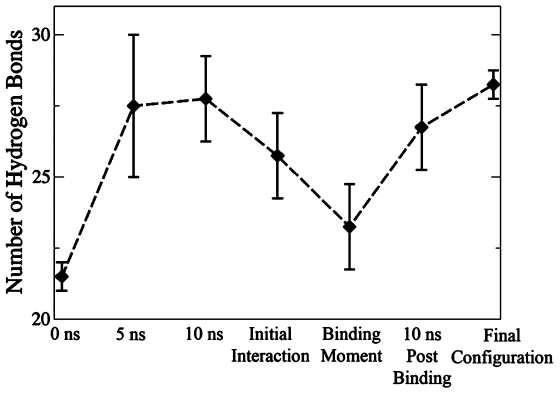

Figure 12. Average number of hydrogen bonds at significant times observed in the multiple peptide−aptamer binding simulations. The average number of hydrogen bonds is shown as symbols along with corresponding variations.

number of hydrogen bonds as the system stabilizes. The initial interaction with the peptide causes a decrease in the number of hydrogen bonds in the aptamer. The binding event triggered by the arginine residue causes the distruption of the hydrogen bonds in the open ends of the aptamer structure. This is evident from the initial reduction in the average number of hydrogen bonds, as shown in Figure 12. However, after the binding the number of hydrogen bonds gradually increases as the aptamer structure reorganizes to a stable confirmation. Toward the end of the simulations the variation within the number of hydrogen bonds in the aptamer structure was found to be minimal. This indicated that the final binding combination in all the simulations obtains a similar compact binding structure.

In addition to intramolecular hydrogen bonding there is also formation and dissolution of hydrogen bonds between the individual molecules and the solvent. Figure 13 shows the average number of hydrogen bonds between the biomolecules and solvent. More importantly, we observe, after the binding event, there is a decrease in the number of hydrogen bonds between the peptide, aptamer, and water. This phenomena is more prevalent between the peptide and water as evident from Figure 13B.

We observe that the interactions between the arginine residue and the 13th thymine nucleotide are present throughout all MUC1-G peptide−aptamer complex simulations. Figure 14 highlights the hydrogen bonds present between the atoms of arginine and 13th thymine nucleotide in the final configuration for each MUC1-G peptide−aptamer complex. Consistently the hydrogen bonds are present between the arginine residue and the 13th nucleotide of the aptamer. The final configuration of the MUC1-G_3 peptide−aptamer complex also showed proline in addition to the arginine interacting with the 13th thymine nucleotide.

A detailed analysis of hydrogen bond formation between the atoms within the multiple MUC1-G binding complexes is presented next. In each case hydrogen bonds are formed between the guanidino nitrogen atoms of the arginine residue and the phosphate oxygen atoms from the 13th nucleotide. Interaction between these atoms establishes a stable peptide−aptamer complex. Further, MUC1-G_3 complex shows a consistent bond between the oxygen of the 13th thymine nucleotide base and the nitrogen of the proline (as shown in Figure 14D). Key prevalent atoms that form the hydrogen bonds between the arginine and 13th thymine residues present in the binding complex in each case of MUC1-G simulations is summarized below.

MUC1-G: Arginine-5 side chain NE with the thymine-13 side chain O1P; arginine-5 side chain NH2 with the thymine-13 side chain O1P; arginine-5 side chain NH1 with the thymine-13 side chain O1P

MUC1-G_1: Arginine-5 side chain NE with the thymine-13 side chain O2P; arginine-5 side chain NH2 with the thymine-13

DOI: 10.1021/acs.jpcb.5b02483
J. Phys. Chem. B XXXX, XXX, XXX−XXX

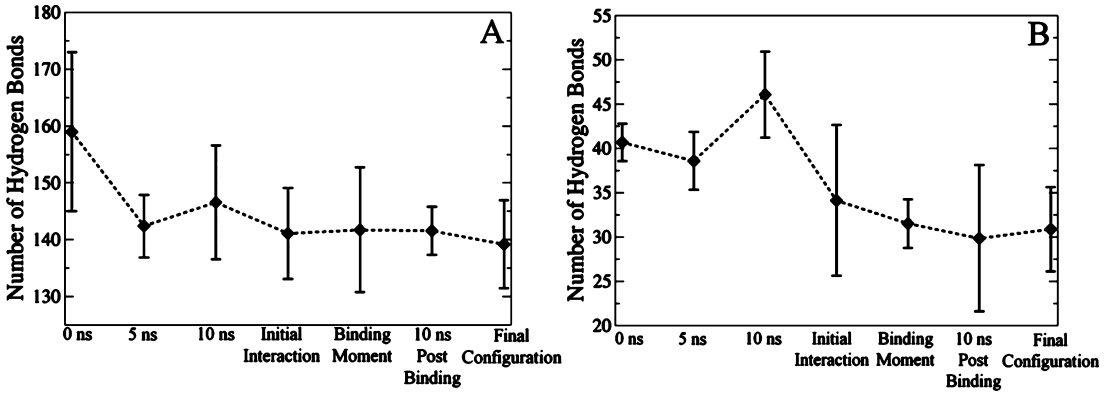

Figure 13. Number of hydrogen bonds between peptide−aptamer molecules with solvent at significant times in the binding simulations. The average values are shown as symbols along with corresponding variations. (A) Number of hydrogen bonds formed between the aptamer and water and (B) number of hydrogen bonds formed between the peptide and water. As can be seen from the figures, number of hydrogen bonds decrease after the binding event.

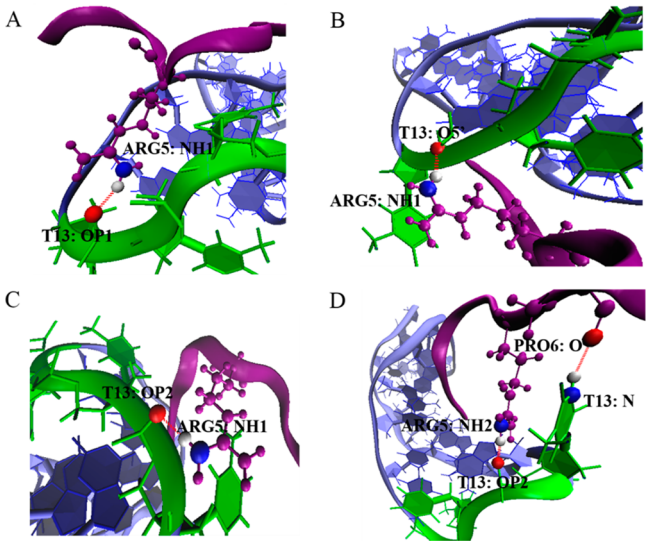

Figure 14. Final snapshots of MUC1-G peptide−aptamer complex from four different simulations are shown. The hydrogen bonds between the peptide and aptamer molecules are highlighted. (A) MUC1-G, (B) MUC1-G_1, (C) MUC1-G_2, and (D) MUC1-G_3.

side chain O2P; arginine-5 side chain NH1 with the thymine-13 side chain O2P

MUC1-G_2: Arginine-5 side chain NH1 with the thymine-13 side chain OP2; arginine-5 side chain NH1 with the thymine-13 side chain P; arginine-5 main chain N with the thymine-13 side chain O4

MUC1-G_3: Arginine-5 side chain NH1 with the thymine-13 side chain O2P; arginine-5 side chain NH1 with the thymine-13 side chain O2P; arginine-5 side chain NH1 with the thymine-13 side chain O5′

DISCUSSION

MD analysis of individual molecules established the stability of aptamer and peptide molecules in the solvent. Multiple simulations with MUC1 peptide and the anti-MUC1 aptamer showed temporary association of these molecules. In particular, we observed that this association occurs at the 5′ and 3′ end region. However, longer time duration analysis revealed peptide reorientation, followed by subsequent separation of these molecules. This weak association between the MUC1 peptide and aptamer was due to the increased flexibility of the peptide backbone as indicated by the structural analysis. Binding atom distance analysis during the brief association fell below 0.45 nm. However, this distance continued to increase with an average value of 0.6 nm which indicates that the MUC1 peptide and aptamer are not in a bound state; no sustained binding can be inferred in all cases.

Multiple simulations showed that the MUC1-G combination consistently interacts with the loop region of the aptamer and binds with that specific region showing a clear sustained binding in all MUC1-G peptide−aptamer cases. The arginine residue of the peptide initiated the interaction with the aptamer. Throughout binding the arginine residue consistently interacted with the 13th thymine nucleotide of the aptamer in all MUC1-G peptide−aptamer simulations. In each simulation a successful binding was observed with a binding time that differed in each case. Binding was further confirmed by calculating the distance between the atoms in the binding region for all MUC1-G combinations studied. This distance was found to remain consistently lower than a value of 0.45 nm after binding which implies that the MUC1-G peptide and aptamer are noncovalently bound and remained in sustained binding state. It is important to note that such sustained binding is required for successful and repeatable biosensor detection mechanisms.

Detailed structural analysis of the multiple MUC1-G peptide−aptamer simulations showed that the aptamer structure is altered during the binding process. This was evident from the changes in the number of hydrogen bonds within the aptamer as it interacted with the peptide. In particular, the hydrogen bonds within the aptamer structure showed distinct changes during its binding with the MUC1-G peptide. Upon binding with the peptide the aptamer internal structure is significantly altered, as the hydrogen bonds holding the helix and open ends together are disrupted resulting in a decrease in the number of hydrogen bonds. As the binding continued, the aptamer tries to reestablish its hydrogen bonds by forming a stable peptide−aptamer binding complex. The solvent environment plays an important role in the formation of stable aptamer binding complexes.[66] Hydrogen bonds formed between the water and MUC1-G peptide−aptamer complexes provide additional insight into the role of the solvent on MUC1-G peptide aptamer binding. After binding event, the number of hydrogen bonds between the water and peptide−

DOI: 10.1021/acs.jpcb.5b02483
J. Phys. Chem. B XXXX, XXX, XXX−XXX

aptamer molecules is found to be reduced. Recent studies of aptamer−protein binding showed that the entropy increases due to dissolution of hydrogen bonds between the water and biomolecules in the system, further driving the binding event.[67] For MUC1-G this phenomena is reflected in the reduction in bonds between the molecules and water and is driven by the interaction and binding of the peptide and aptamer.

We find successful and sustained binding in all the MUC1-G peptide−aptamer complex simulations. Further, we observe these binding complexes were initiated by the arginine residue and stabilized by the formation of hydrogen bonds with 13th thymine nucleotide (Figure 12). A detailed analysis indicated that the nitrogen atoms of the arginine side chain and the phosphate oxygen atoms of the 13th thymine nucleotide specifically involved in the formation of hydrogen bonds. In the MUC1-G_3 complex, additional hydrogen bonding between the nitrogen of the 13th thymine nucleotide base and the oxygen of the sixth proline residue of the peptide was found to further support the binding (see Supporting Information). This interaction with proline can be explicated by the unique arc-like configuration of the peptide around the 13th thymine residue as observed in Figure 7. Structurally, looking at the individual comparison of the peptides shows the difference in major contributing factor between the MUC1 and MUC1-G peptides is the addition of the glycine residue. The MUC1 and MUC1-G peptides have a great presence of arginine and proline residues. Arginine has a positive charge which aids stable interactions with the DNA. Proline is known to play an important role in molecular recognition.[68] Structurally, proline presence leads to a low conformational flexibility.[69,70] Glycine is the mirror opposite and has a high conformational flexibility due to its hydrogen side chain. While both peptides show the ability to interact with the DNA aptamer, glycine's conformational flexibility is a noted contributing factor in the stable binding event between the MUC1-G peptide and aptamer.

A previous wet lab experimental study by Ferreira et al. indicated a strong binding of anti-MUC1 aptamer and MUC1-G peptide.[39] By using surface plasmon resonance imaging (SPRi) they found that the combination of MUC1-G peptide and anti-MUC1 aptamer showed a relatively faster association compared to other mucin 1 peptides. The MUC1-G peptide−aptamer complex was shown to be a stronger binding combination with a low dissociation constant. In their work,[39] alternative combinations of MUC1 peptide and anti-MUC1 aptamer were also studied and were consistently shown to be weaker binding combinations compared to the MUC1-G peptide and aptamer. This concurs well with our multiple simulation MD modeling analysis results that consistently showed a stronger binding between the MUC1-G peptide and anti-MUC1 aptamer, and only weaker interaction in the case of MUC1 peptide−aptamer.

The present study showed that the computational modeling can be effectively used to determine the binding behavior, location and orientation for peptide−aptamer binding combinations. Such findings have important implications for aptamer based biosensor development. In practice, the aptamers are immobilized on the biosensor surface.[35,71,72] To optimize sensor efficiency there is a need to immobilize the aptamers for maximum access to their binding region. Aptamers and their target ligands (like the MUC1-G peptide) can have multiple binding sites. Detailed insights such as the binding conformation, binding location and relative orientation of the peptide−aptamer combination can be obtained from MD modeling analysis of peptide−aptamer complex as discussed in the present work. By identifying these specific binding region and the aptamer orientation within the binding complex, it is possible to immobilize the aptamer within a biosensor in such a manner that will provide greater accessibility to the binding region.[35,36] This in turn aids in efficient biomarker detection within a biosensor.

CONCLUDING REMARKS

Computational modeling and molecular dynamics simulations could provide effective means to study and understand complex biological phenomenon such as biomarker-aptamer binding combinations. In this work extensive molecular dynamics simulations of the anti-MUC1 aptamer with multiple MUC1 and MUC1-G peptide binding combinations were conducted and analyzed using GROMACS. MUC1-G peptide, a variant of MUC1 peptide was generated by adding a glycine residue. After exploring the structure and dynamics of individual molecules, aptamer binding with MUC1 peptide and MUC1-G peptide were modeled and analyzed via MD extensively. Multiple simulation results showed that the common peptide sequence APDTRPAP, in particular the arginine residue plays an important role in facilitating binding. The addition of residues like glycine, in the MUC1-G peptide, help maintain binding to the anti-MUC1 aptamer. The occurrence of binding events was monitored by calculating the distance between peptide and aptamer molecules. We find that the distance between the atoms within the binding region decreased due to binding. The formation of the binding complex was further supported by the calculation of the number of hydrogen bonds within the aptamer structure. Multiple simulations demonstrated that the MUC1-G binding event occurs consistently in the loop region of the aptamer thus providing a sustained peptide−aptamer binding in the case of MUC1-G peptide−aptamer complex. Simulations reveal that the arginine residue of the peptide played a key role in forming the peptide−aptamer binding.

The simulation results of the present study demonstrate that even small changes in peptide sequence can impact binding. Simulations also reveal a natural progression of the entire aptamer and peptide binding event in solvent. Insights from this study could aid in biosensor developments by providing pointers on specificities of binding such as aptamer orientation and location that are critical to enhance detection mechanisms. Further insights into such complex phenomena can be obtained by studying additional variations of mucin 1 peptide−aptamer complexes. Though we have identified major binding factors, further insights into other possible contributing factors can be obtained by systematically studying series of binding and nonbinding complexes, which is, however, computationally highly challenging. Additional information can also be acquired through quantum mechanics simulations of the binding sites. Such expansive research would be computationally heavy but could provide additional insights. Concurrently, in the present study, the peptide was presented without a blocking agent or a cap. As capping can have varied effects on the simulation[73,74] we chose to perform these foundational simulations without a capping agent. Further simulation is needed to specifically determine the effects of capping for this binding combination, and is not considered in the present work.

The methods used in this study can be adapted to analyze other biomarker-aptamer combinations. The insights obtained from this study may also be used to simplify the complex and involved SELEX process. However, this involves studying a

DOI: 10.1021/acs.jpcb.5b02483
J. Phys. Chem. B XXXX, XXX, XXX−XXX

substantial number of biomarker-aptamer combinations which would be near impossible, and computationally expensive to study with the computational methods based on atomistic details. For this purpose, we intend to develop intermediate coarse-grain models, which are known to increase the simulation efficiency by decreasing the number of degrees of freedom.[75,76] Further work in this direction is under progress.

■ ASSOCIATED CONTENT

Ⓢ Supporting Information

Additional figures and data to aid demonstration of MUC1-G peptide−aptamer binding as well as analysis and comparison of MUC1 and MUC1-G peptide−aptamer simulations. The Supporting Information is available free of charge on the ACS Publications website at DOI: 10.1021/acs.jpcb.5b02483.

■ AUTHOR INFORMATION

Corresponding Author

*(R.V.M.) E-mail: rvmohan@ncat.edu.

Notes

The authors declare no competing financial interest.

■ ACKNOWLEDGMENTS

This work was supported in part by the U.S. Army Research Office via Award/Contract No. W911NF-11-1-0168. We thank Dr. M. Sandros for scientific discussions during the course of this work. We would like to acknowledge the use of high performance computational facilities at the North Carolina State A&T University during the course of the present study.

■ REFERENCES

(1) Jain, K. K. *The Handbook of Biomarkers*; Springer: New York, 2010.
(2) Scognamiglio, V. Nanotechnology in glucose monitoring: Advances and challenges in the last 10 years. *Biosens. Bioelectron.* **2013**, *47*, 12−25.
(3) Chang, K.; Pi, Y.; Lu, W.; Wang, F.; Pan, F.; Li, F.; Jia, S.; Shi, J.; Deng, S.; Chen, M. Label-free and high-sensitive detection of human breast cancer cells by aptamer-based leaky surface acoustic wave biosensor array. *Biosens. Bioelectron.* **2014**, *60*, 318−324.
(4) Ma, F.; Ho, C.; Cheng, A. K. H.; Yu, H.-Z. Immobilization of redox-labeled hairpin DNA aptamers on gold: Electrochemical quantitation of epithelial tumor marker mucin 1. *Electrochim. Acta* **2013**, *110*, 139−145.
(5) Shum, K. T.; Zhou, J.; Rossi, J. J. Nucleic acid aptamers as potential therapeutic and diagnostic agents for lymphoma. *J. Cancer Ther.* **2013**, *4*, 872−890.
(6) Malic, L.; Sandros, M. G.; Tabrizian, M. Designed biointerface using near-infrared quantum dots for ultrasensitive surface plasmon resonance imaging biosensors. *Anal. Chem.* **2011**, *83*, 5222−9.
(7) Bohunicky, B.; Mousa, S. A. Biosensors: The new wave in cancer diagnosis. *Nanotechnol., Sci. Appl.* **2011**, *4*, 1−10.
(8) Turner, A. P. Biosensors: Sense and sensibility. *Chem. Soc. Rev.* **2013**, *42*, 3184−3196.
(9) Hu, M.; Zhang, K. The application of aptamers in cancer research: An up-to-date review. *Future Oncol.* **2013**, *9*, 369−376.
(10) Ahmed, M. U.; Saaem, I.; Wu, P. C.; Brown, A. S. Personalized diagnostics and biosensors: A review of the biology and technology needed for personalized medicine. *Crit. Rev. Biotechnol.* **2013**, *34*, 180−196.
(11) Bertucci, C.; De Simone, A. Optical biosensors and applications to drug discovery and development in cancer research. In *Biosensors and Cancer*; Preedy, V. R., Patel, V. B., Eds.; CRC Press: Boca Raton, FL, 2012; pp 321−336.
(12) Baruch, A.; Hartmann, M.-l.; Yoeli, M.; Adereth, Y.; Greenstein, S.; Stadler, Y.; Skornik, Y.; Zaretsky, J.; Smorodinsky, N. I.; Keydar, I.; et al. The breast cancer-associated MUC1 gene generates both a receptor and its cognate binding protein. *Cancer Res.* **1999**, *59*, 1552−1561.
(13) Gendler, S. J. MUC1, the renaissance molecule. *J. Mammary Gland Biol. Neoplasia* **2001**, *6*, 339−353.
(14) Dokurno, P.; Bates, P. A.; Band, H. A.; Stewart, L. M. D.; Lally, J. M.; Burchell, J. M.; Taylor-Papadimitriou, J.; Snary, D.; Sternberg, M. J. E.; Freemont, P. S. Crystal structure at 1.95 Å resolution of the breast tumour-specific antibody SM3 complexed with its peptide epitope reveals novel hypervariable loop recognition. *J. Mol. Biol.* **1998**, *284*, 713−728.
(15) Taylor-Papadimitriou, J.; Burchell, J. M.; Plunkett, T.; Graham, R.; Correa, I.; Miles, D.; Smith, M. MUC1 and the immunobiology of cancer. *J. Mammary Gland Biol. Neoplasia* **2002**, *7*, 209−221.
(16) Kirnarsky, L.; Prakash, O.; Vogen, S. M.; Nomoto, M.; Hollingsworth, M. A.; Sherman, S. Structural effects of O-glycosylation on a 15-residue peptide from the mucin (MUC1) core protein. *Biochemistry* **2000**, *39*, 12076−12082.
(17) von Mensdorff-Pouilly, S.; Gourevitch, M. M.; Kenemans, P.; Verstraeten, A. A.; van Kamp, G. J.; Kok, A.; van Uffelen, K.; Snijdewint, F. G. M.; Paul, M. A.; Meijer, S.; et al. An enzyme-linked immunosorbent assay for the measurement of circulating antibodies to polymorphic epithelial mucin (MUC1). *Tumor Biol.* **1998**, *19*, 186−195.
(18) Pichinuk, E.; Benhar, I.; Jacobi, O.; Chalik, M.; Weiss, L.; Ziv, R.; Sympson, C.; Karwa, A.; Smorodinsky, N. I.; Rubinstein, D. B.; et al. Antibody targeting of cell-bound MUC1 SEA domain kills tumor cells. *Cancer Res.* **2012**, *72*, 3324−3336.
(19) Hamanaka, Y.; Suehiro, Y.; Fukui, M.; Shikichi, K.; Imai, K.; Hinoda, Y. Circulating anti-MUC1 IgG antibodies as a favorable prognostic factor for pancreatic cancer. *Int. J. Cancer* **2003**, *103*, 97−100.
(20) Strehlitz, B.; Nikolaus, N.; Stoltenburg, R. Protein detection with aptamer biosensors. *Sensors* **2008**, *8*, 4296−4307.
(21) Erickson, D.; Mandal, S.; Yang, A.; Cordovez, B. Nanobiosensors: Optofluidic, electrical and mechanical approaches to biomolecular detection at the nanoscale. *Microfluid. Nanofluid.* **2008**, *4*, 33−52.
(22) Han, K.; Liang, Z.; Zhou, N. Design strategies for aptamer-based biosensors. *Sensors* **2010**, *10*, 4541−4557.
(23) Wang, J. From DNA biosensors to gene chips. *Nucleic Acid Res.* **2000**, *28*, 3011−3016.
(24) Song, S.; Wang, L.; Li, J.; Fan, C.; Zhao, J. Aptamer-based biosensors. *TrAC, Trends Anal. Chem.* **2008**, *27*, 108−117.
(25) McCauley, T. G.; Hamaguchi, N.; Stanton, M. Aptamer-based biosensor arrays for detection and quantification of biological macromolecules. *Anal. Biochem.* **2003**, *319*, 244−250.
(26) He, P.; Oncescu, V.; Lee, S.; Choi, I.; Erickson, D. Label-free electrochemical monitoring of vasopressin in aptamer-based microfluidic biosensors. *Anal. Chim. Acta* **2013**, *759*, 74−80.
(27) Palchetti, I.; Mascini, M. Aptamer-based biosensors for cancer studies. In *Biosensors and Cancer*; Preedy, V. R., Patel, V. B., Eds.; CRC Press: Boca Raton, FL, 2012; pp 85−100.
(28) Clark, S. L.; Remcho, V. T. Aptamers as analytical reagents. *Electrophoresis* **2002**, *23*, 1335−1340.
(29) Stoltenburg, R.; Reinemann, C.; Strehlitz, B. SELEX–A (r)evolutionary method to generate high-affinity nucleic acid ligands. *Biomol. Eng.* **2007**, *24*, 381−403.
(30) Tuerk, C.; Gold, L. Systematic evolution of ligands by exponential enrichment: RNA ligands to bacteriophage T4 DNA polymerase. *Science* **1990**, *249*, 505−510.
(31) Kolmodin, L. A.; Birch, D. E. Polymerase chain reaction. Basic principles and routine practice. *Methods Mol. Biol.* **2002**, *192*, 3−18.
(32) Bartlett, J. S.; Stirling, D. A Short history of the polymerase chain reaction. In *PCR Protocols*; Bartlett, J. S., Stirling, D., Eds.; Humana Press: New York, 2003; Vol. *226*; pp 3−6.

DOI: 10.1021/acs.jpcb.5b02483
J. Phys. Chem. B XXXX, XXX, XXX−XXX

(33) Saiki, R.; Gelfand, D.; Stoffel, S.; Scharf, S.; Higuchi, R.; Horn, G.; Mullis, K.; Erlich, H. Primer-directed enzymatic amplification of DNA with a thermostable DNA polymerase. *Science* **1988**, *239*, 487−491.
(34) Chai, C.; Xie, Z.; Grotewold, E. SELEX (Systematic Evolution of Ligands by EXponential Enrichment), as a powerful tool for deciphering the protein-DNA interaction space. *Methods Mol. Biol.* **2011**, *754*, 249−58.
(35) Wan, Y.; Su, Y.; Zhu, X.; Liu, G.; Fan, C. Development of electrochemical immunosensors towards point of care diagnostics. *Biosens. Bioelectron.* **2013**, *47*, 1−11.
(36) Ziegler, C.; Göpel, W. Biosensor development. *Curr. Opin. Chem. Biol.* **1998**, *2*, 585−591.
(37) Hosseini, S.; Ibrahim, F.; Djordjevic, I.; Koole, L. H. Recent advances in surface functionalization techniques on polymethacrylate materials for optical biosensor applications. *Analyst* **2014**, *139*, 2933−2943.
(38) Chen, H.; Huang, J.; Lee, J.; Hwang, S.; Koh, K. Surface plasmon resonance spectroscopic characterization of antibody orientation and activity on the calixarene monolayer. *Sens. Actuators, B* **2010**, *147*, 548−553.
(39) Ferreira, C. S.; Matthews, C. S.; Missailidis, S. DNA aptamers that bind to MUC1 tumour marker: design and characterization of MUC1-binding single-stranded DNA aptamers. *Tumor Biol.* **2006**, *27*, 289−301.
(40) Nguyen, T. H. T.; Liu, Z.; Moore, P. B. Molecular dynamics simulations of homo-oligomeric bundles embedded within a lipid bilayer. *Biophys. J.* **2013**, *105*, 1569−1580.
(41) Kim, S.; Lee, J.; Lee, S. J.; Lee, H. J. Ultra-sensitive detection of IgE using biofunctionalized nanoparticle-enhanced SPR. *Talanta* **2010**, *81*, 1755−1759.
(42) Ozsoz, M. S. *Electrochemical DNA Biosensors*; Pan Stanford: Singapore, 2012.
(43) Cheng, X.; Ivanov, I. Molecular dynamics. In *Computational Toxicology*; Reisfeld, B., Mayeno, A. N., Eds.; Humana Press: New York, 2012; Vol. *929*; pp 243−285.
(44) Ivanov, I.; Chapados, B. R.; McCammon, J. A.; Tainer, J. A. Proliferating cell nuclear antigen loaded onto double-stranded DNA: Dynamics, minor groove interactions and functional implications. *Nucleic Acids Res.* **2006**, *34*, 6023−6033.
(45) Palermo, G.; Rothlisberger, U.; Cavalli, A.; De Vivo, M. Computational insights into function and inhibition of fatty acid amide hydrolase. *Eur. J. Med. Chem.* **2015**, *91*, 15−26.
(46) Rhinehardt, K.; Mohan, R.; Srinivas, G.; Kelkar, A. Computational modeling of peptide - Aptamer binding in biosensor applications. *Int. J. Biosci., Biochem. Bioinf.* **2013**, *3*, 639−642.
(47) *The PyMOL Molecular Graphics System*, version 1.3; Schrödinger, LLC: New York, 2010.
(48) Hornak, V.; Abel, R.; Okur, A.; Strockbine, B.; Roitberg, A.; Simmerling, C. Comparison of multiple Amber force fields and development of improved protein backbone parameters. *Proteins: Struct., Funct., Bioinf.* **2006**, *65*, 712−725.
(49) Van Der Spoel, D.; Lindahl, E.; Hess, B.; Groenhof, G.; Mark, A. E.; Berendsen, H. J. C. GROMACS: Fast, flexible, and free. *J. Comput. Chem.* **2005**, *26*, 1701−1718.
(50) Lange, O. F.; van der Spoel, D.; de Groot, B. L. Scrutinizing molecular mechanics force fields on the submicrosecond timescale with NMR Data. *Biophys. J.* **2010**, *99*, 647−655.
(51) Wickstrom, L.; Okur, A.; Simmerling, C. Evaluating the performance of the ff99SB force field based on NMR scalar coupling data. *Biophys. J.* **2009**, *97*, 853−856.
(52) Kumar, P. S.; Mukherjee, A.; Hazra, A. Theoretical study of structural changes in DNA under high external hydrostatic pressure. *J. Phys. Chem. B* **2015**, *119*, 3348−3355.
(53) Junlang, C.; Liang, C.; Yu, W.; Shude, C. Molecular dynamics simulations of the adsorption of DNA segments onto graphene oxide. *J. Phys. D: Appl. Phys.* **2014**, *47*, 505401.
(54) Berendsen, H. J. C.; van der Spoel, D.; van Drunen, R. GROMACS: A message-passing parallel molecular dynamics implementation. *Comput. Phys. Commun.* **1995**, *91*, 43−56.
(55) Hess, B.; Kutzner, C.; van der Spoel, D.; Lindahl, E. GROMACS 4: Algorithms for highly efficient, load-balanced, and scalable molecular simulation. *J. Chem. Theory Comput.* **2008**, *4*, 435−447.
(56) Nosé, S.; Klein, M. L. Constant pressure molecular dynamics for molecular systems. *Mol. Phys.* **1983**, *50*, 1055−1076.
(57) Humphrey, W.; Dalke, A.; Schulten, K. VMD: Visual molecular dynamics. *J. Mol. Graphics* **1996**, *14*, 33−38.
(58) Carugo, O. How root-mean-square distance (r.m.s.d.) values depend on the resolution of protein structures that are compared. *J. Appl. Crystallogr.* **2003**, *36*, 125−128.
(59) de Gennes, P.-G. *Scaling Concepts in Polymer Physics*; Cornell University Press: Ithaca, NY, 1979.
(60) Berg, J. M.; Deis, F. H.; Tymoczko, J. L.; Stryer, L.; Gerber, N. C.; Gumport, R.; Koeppe, R. E. *Biochemistry Student Companion*; W. H. Freeman: New York, 2011.
(61) Farrell, S.; Taylor, L. *Experiments in Biochemistry: A Hands-On Approach*; Cengage Learning: Boston, MA, 2005.
(62) Schalley, C. A. *Analytical Methods in Supramolecular Chemistry*: *Vol. 1*; Wiley-VCH Verlag GmbH & Company KGaA: Weinheim, Germany, 2012.
(63) Bondi, A. Van der Waals volumes and radii. *J. Phys. Chem.* **1964**, *68*, 441−451.
(64) Pal, S.; Maiti, P. K.; Bagchi, B. Exploring DNA groove water dynamics through hydrogen bond lifetime and orientational relaxation. *J. Chem. Phys.* **2006**, *125*, 234903.
(65) Van der Spoel, D.; Lindahl, E.; Hess, B.; van Buuren, A. R.; Apol, E.; Meulenhoff, P. J.; Tieleman, D. P.; Sijbers, A. L. T. M.; Feenstra, K. A.; van Drunen, R.; Berendsen, H. J. C. Gromacs User Manual version 4.5.4, www.gromacs.org (2010).
(66) Bernard Da Costa, J.; Dieckmann, T. Entropy and Mg^{2+} control ligand affinity and specificity in the malachite green binding RNA aptamer. *Mol. BioSyst.* **2011**, *7*, 2156−2163.
(67) Hayashi, T.; Oshima, H.; Mashima, T.; Nagata, T.; Katahira, M.; Kinoshita, M. Binding of an RNA aptamer and a partial peptide of a prion protein: Crucial importance of water entropy in molecular recognition. *Nucleic Acids Res.* **2014**, *42*, 6861−6875.
(68) Betts, M. J.; Russell, R. B. Amino acid properties and consequences of substitutions. In *Bioinformatics for Geneticists*; John Wiley & Sons, Ltd.: Chichester, U.K., 2003; pp 289−316.
(69) Tramontano, A. *Protein Structure Prediction: Concepts and Applications*; Wiley-VCH: Weinheim, Germany, 2006.
(70) Buxbaum, E. *Fundamentals of Protein Structure and Function*; Springer US: New York, 2007.
(71) Vance, S. A.; Sandros, M. G. Zeptomole detection of C-reactive protein in serum by a nanoparticle amplified surface plasmon resonance imaging aptasensor. *Sci. Rep.* **2014**, *4*, 5129.
(72) Pilolli, R.; Monaci, L.; Visconti, A. Advances in biosensor development based on integrating nanotechnology and applied to food-allergen management. *TrAC, Trends Anal. Chem.* **2013**, *47*, 12−26.
(73) Andreasen, M.; Skeby, K. K.; Zhang, S.; Nielsen, E. H.; Klausen, L. H.; Frahm, H.; Christiansen, G.; Skrydstrup, T.; Dong, M.; Schiott, B.; Otzen, D. The importance of being capped: Terminal capping of an amyloidogenic peptide affects fibrillation propensity and fibril morphology. *Biochemistry* **2014**, *53*, 6968−6980.
(74) Cino, E. A.; Choy, W. Y.; Karttunen, M. Comparison of secondary structure dormation using 10 different force fields in microsecond molecular dynamics simulations. *J. Chem. Theory Comput.* **2012**, *8*, 2725−2740.
(75) Marrink, S. J.; Risselada, H. J.; Yefimov, S.; Tieleman, D. P.; de Vries, A. H. The MARTINI force field: Coarse grained model for biomolecular simulations. *J. Phys. Chem. B* **2007**, *111*, 7812−7824.
(76) Sim, A. Y. L.; Minary, P.; Levitt, M. Modeling nucleic acids. *Curr. Opin. Struct. Biol.* **2012**, *22*, 273−278.

DOI: 10.1021/acs.jpcb.5b02483
J. Phys. Chem. B XXXX, XXX, XXX−XXX